Clay Dispersion Assessment via FT-Rheology for Polypropylene/Clay Nanocomposites Fabricated by Electric Field

Journal:	*ACS Applied Polymer Materials*
Manuscript ID	ap-2023-01104r.R2
Manuscript Type:	Article
Date Submitted by the Author:	10-Aug-2023
Complete List of Authors:	Kim, Mingeun ; Korea Research Institute of Chemical Technology Kim, Min; School of Chemical and Biomolecular Engineering, Pusan National University Myung, Jin Suk ; Korea Research Institute of Chemical Technology Salehiyan, Reza; Edinburgh Napier University Choi, Woo Jin; Korea Research Institute of Chemical Technology, Hyun, Kyu; Pusan National University, School of Chemical Engineering

Submitted to "***ACS applied polymer materials***"

Clay Dispersion Assessment via FT-Rheology for Polypropylene/Clay Nanocomposites Fabricated by Electric Field

Mingeun Kim[a,b], Min Chan Kim[a], Jin Suk Myung[b], Reza Salehiyan[c], Woo Jin Choi[b], and Kyu Hyun[a,*]

[a]*School of Chemical Engineering, Pusan National University, Busan, 46241, Republic of Korea*

[b]*Chemical Materials Solutions Center, Korea Research Institute of Chemical Technology (KRICT), Daejeon, 34114, Republic of Korea*

[c]*School of Computing, Engineering and Built Environment, Edinburgh Napier University, Edinburgh, EH10 5DT, United Kingdom*

*Email: kyuhyun@pusan.ac.kr

ABSTRACT: Nonlinear viscoelastic parameters obtained from the large amplitude oscillatory shear (LAOS) test have widely received attention in polymer nanocomposite (PNC) characterization. Previously, we reported that nonlinear parameters, Q_0 and NLR (nonlinear-linear viscoelastic ratio) from FT-rheology, better-characterized filler dispersion in PNCs than the linear viscoelastic parameters of small amplitude oscillatory shear (SAOS) test and concluded that nonlinear parameters could detect interfacial area much more sensitively than linear parameters. [*Macromolecules* **2019**, *52*, 8604]. To confirm this, we systemically manipulated the clay dispersion states of polypropylene (PP)/clay PNCs in this study by applying an electric field (EF). An EF can easily manipulate the dispersion quality of clays, i.e., tactoid, intercalation, and exfoliation in a polymer matrix, by controlling the application time. The clay dispersion was examined using the rheological properties of SAOS and LAOS tests. The linear viscoelastic properties ($|G^*|$) from the SAOS test increased monotonically with increasing clay content and EF application time. In contrast, the nonlinear rheological properties (Q_0) by FT-rheology from the LAOS test exhibited more prominent and sensitive growth. When the concentration of clay increased without EF application (φ = 1,3, and 5wt%), $|G^*|(\varphi)/|G^*|(\mathrm{PP})$ increased from 1 to 2.05 whereas $Q_0(\varphi)/Q_0(\mathrm{PP})$ increased from 1 to 22.8. In 5wt% clay PNC, EF was applied in increments of 3,7,10,20, and 30min. With increasing EF application time, $|G^*|(5\mathrm{wt\%})/|G^*|(\mathrm{PP})$ increased from 1 to 3.24, while $Q_0(5\mathrm{wt\%})/Q_0(\mathrm{PP})$ increased significantly from 1 to 13,540.

KEYWORDS: *polymer nanocomposite, filler dispersion, electric field, FT-rheology, large amplitude oscillatory shear (LAOS)*

1. INTRODUCTION

The interest in polymer composite materials has focused on the nanoscale since the Toyota research group synthesized polyamide 6 (PA6)/clay nanocomposite.[1] Superior property enhancements in polymer nanocomposites (PNCs) could be achieved with less filler content than conventional polymer (micro-) composites, thanks to the larger surface area of nano-fillers. Hence, numerous studies have been conducted to develop PNC materials for filler dispersion enhancement. Several methods are derived mainly from the intercalation of polymers or pre-polymer from solution, in situ intercalative polymerization, and melt intercalation methods.[2] The melt intercalation method, i.e., melt-compounding of a polymer matrix and filler, is mainly interested in the industrial as well as the academic with the advantage of solvent-free and mass-production.[2]

Measuring the filler dispersion in PNCs is challenging because of the complex internal structure. As thinner and finer particles are dispersed in a polymer matrix, the techniques for characterizing the filler dispersion must also be improved to understand and manage PNC materials. Therefore, various methods are used cooperatively to analyze the state of nanoparticle dispersions in a polymer matrix, e.g., transmission electron microscopy (TEM), scanning electron microscopy (SEM), X-ray diffraction (XRD), mechanical tests, dielectric spectroscopy, and rheology. Among them, rheological measurements have been adopted widely to evaluate the filler dispersion in the melt state because of its high sensitivity to variations in the microstructure.[3–11]

A small amplitude oscillatory shear (SAOS) test is a rheological measurement used widely to indicate the morphological state of PNCs. The relevant parameters measured on a wide frequency range are used to understand PNCs. For example, the storage modulus (G') represents morphological evolution by lowering the scaling behavior with an exponent (n) at the terminal region ($G' \sim \omega^n$) corresponding to the low-frequency range.[6] The exponent n decreases in low frequencies with filler dispersion enhancement. Lertwimolnun and Vergnes[7] examined the morphological evolution of polypropylene (PP)/clay PNCs compatibilized by maleic anhydride-grafted polypropylene (MAPP), with $G'(\omega)$ and complex viscosity ($|\eta^*(\omega)|$). They exhibited that $G'(\omega)$ and $|\eta^*(\omega)|$ are sensitive to a higher degree of clay exfoliation. The characteristic responses of SAOS parameters for morphological development were

attributed to the solid-like behavior in the low-frequency region, showing identical results. Although SAOS parameters are usually used to characterize the PNC morphology, they sometimes fail for the dispersion of nano-sphere particles in PNC.[8,9,12,13] Kim et al.[8] considered the morphological evaluation for PP/MAPP/clay and PP/silica PNCs, using n ($G'(\omega)$) and $|\eta^*(\omega)|$ in SAOS results. The SAOS parameter for PP/MAPP/clay PNCs agreed well with the TEM observations, whereas those for PP/silica PNCs did not agree. They questioned why the SAOS parameters do not reflect well the morphological information on the filler in PNCs. They suggested that the SAOS parameters include complex internal structure information originating from the filler-matrix and the filler and matrix itself in a complicated manner. Kim et al.[8] used additional parameters to characterize the morphology of PP/silica PNCs, which were from Fourier transform (FT)-rheology, i.e., zero-strain nonlinearity Q_0 suggested by Hyun and Wilhelm[14] and nonlinear-linear viscoelastic ratio (NLR) suggested by Lim et al.[15] These nonlinear rheological parameters showed more sensitive responses to the filler loading and dispersion enhancement for polycaprolactone PNCs.[15] Kim et al.[8] successfully determined the filler dispersion states of PP/silica PNCs and the PP/MAPP/clay using nonlinear parameters from the LAOS test. The actual morphology of PE/silica PNCs was not predicted using SAOS parameters, whereas the nonlinear parameters (Q_0 and NLR from FT-rheology) predicted it well.[9] They reported that growth in nonlinear parameters correlated with the interfacial area between the heterogeneous phases.[8] Based on the above research, we may deduce that nonlinear parameters imply interfacial property quantitatively (i.e., the amount of interfacial area between complex components also can be considered as how much it disperses finely in PNCs).

We applied the electric field (EF) on PP/clay nanocomposite to confirm this. Kim et al.[16] reported a method for improving clay dispersion in PP/clay PNCs on melt-state in a rheometer by applying EF. This experimental setup has the advantage of observing the development of clay dispersions directly by measuring the rheological properties.[16–20] An EF can easily manipulate the dispersion quality of clays, i.e., tactoid (stacked clay platelets), intercalation (polymer chains between clay platelets), and exfoliation (single clay platelets) in a polymer matrix by controlling the application time,[17–19] EF type,[17–19] and strength of the applied EF[17,19,20]. Therefore, electrically activated PP/Clay nanocomposite is an

excellent material system for studying the relationship between nonlinear viscoelastic parameters and dispersion quality. Because clay has a high aspect ratio (length/thickness > 100), the exfoliation hugely increases the interface between clay and polymer.

Therefore, in this study, we systemically manipulated the dispersion states of PP/clay PNCs using an EF application. The interface area between the clay and PP matrix can vary, even with the same clay content, owing to manipulated clay dispersion stated by EF application time. We correlated controlled clay dispersion states and nonlinear parameters (Q_0 and NLR from FT-rheology).

2. EXPERIMENTAL

2.1. Materials. Homopolymer polypropylene (PP, grade: HP562T, M_w = 127,000 g/mol, M_n = 13,000 g/mol, MI = 60 g/10min at 230 ℃ and 2.16 kg, ρ = 0.90 g/cm^3) was provided by Polymirae (Republic of Korea). Dimethyl-hydrogenated tallow ammonium-modified montmorillonite (C20A, Cloisite 20A, ρ = 1.77 g/cm^3) was a donation from BYK (Germany). Material information is summarized in Table S1.

2.2. Sample Preparation. All ingredients for compounding were dried in a vacuum oven at 80 ℃ for 24 hours to eliminate the humidity. Melt compounding was performed in an intensive internal Haake mixer (Thermo Fisher Scientific Inc.) at 180 ℃ for 8 min at a rotor speed of 80 rpm after all ingredients-feeding. Clay was loaded at 1, 3, and 5 weight percentages (wt%) to each PP matrix, called PP/C20A1wt, PP/C20A3wt, and PP/C20A5wt, respectively. The electric field application period (minute) for PP/C20A is denoted behind each specimen, e.g., PP/C20A5wt 10min. All the specimens used are summarized in Table S2.

2.3. Rheological Measurements. All rheological properties were obtained using a strain-controlled rheometer RMS-800 (Rheometrics Inc., USA). In addition, custom-made 25 mm parallel-plate geometries were used to measure the rheological properties and apply the electric field (EF) to the PP/C20A PNCs in situ. EF is alternating current (AC)-type (strength of 1.0 kV/mm and frequency of 60 Hz). The geometry consisted of two major parts: Insulating parts to be docked to the RMS-800 and conducting parts to be connected to the EF application equipment set up and melted PNCs (Figure 1a).

Figure 1b illustrates the mechanism of clay dispersion enhancement under EF application. EF was applied in the time sweep test to the PP/C20A PNCs between 25 mm parallel plates with a 1 mm gap using a function generator and a high voltage amplifier. Only AC was applied here because it was more effective on clay exfoliation than a direct current (DC) EF for the same experimental setup.[17,18] EF application was accomplished using a Tektronix AFG 310 function generator and a Trek 677B high voltage amplifier and was monitored using a Tektronix TDS210 digital oscilloscope. The EF direction was perpendicular to the shear direction. More details on the mechanical setup are described in the initial investigations.[16,19,20]

The time sweep tests were conducted at a frequency of 1 rad/s and a strain amplitude of 0.03 within the linear viscoelastic (LVE) region. At 5 min after running the time sweep test, EF was applied for varying application durations: 3, 7, 10, 20, and 30 min. Subsequently, frequency and strain sweep tests were conducted in series: A frequency range of 0.1–100 rad/s at a strain amplitude of 0.03 for the frequency sweep test and a strain amplitude range of 0.01–5.0 at a frequency of 1 rad/s for the strain sweep test. All rheological measurements were carried out at 170 ℃. Additionally, a frequency sweep test was done after sample loading and before the time sweep test (EF application) to check whether it melted well. The rheological experimental sequence is demonstrated in Figure S1.

The raw data strain and stress as a function of time were acquired from RMS800 to a computer using an analog-digital converting (ADC) card through Bayonet Neill-Concelman (BNC) cables. An ADC card was installed on a computer and recorded raw data with the LabView program (National Instruments, USA). More details about this setup were described by Kim et al.[16] and Hyun et al.[19]

2.4. Morphological Characterizations. Cryo-ultra-microtome was performed using Leica EM UC7 (Leica Microsystems, Germany) at -140 ℃ for the TEM observation. The microtomed specimens were spread on a copper grid. The morphological observation was conducted using FEI Talos F200X (Thermo Fisher Scientific Inc., USA) at an accelerating voltage of 200 kV.

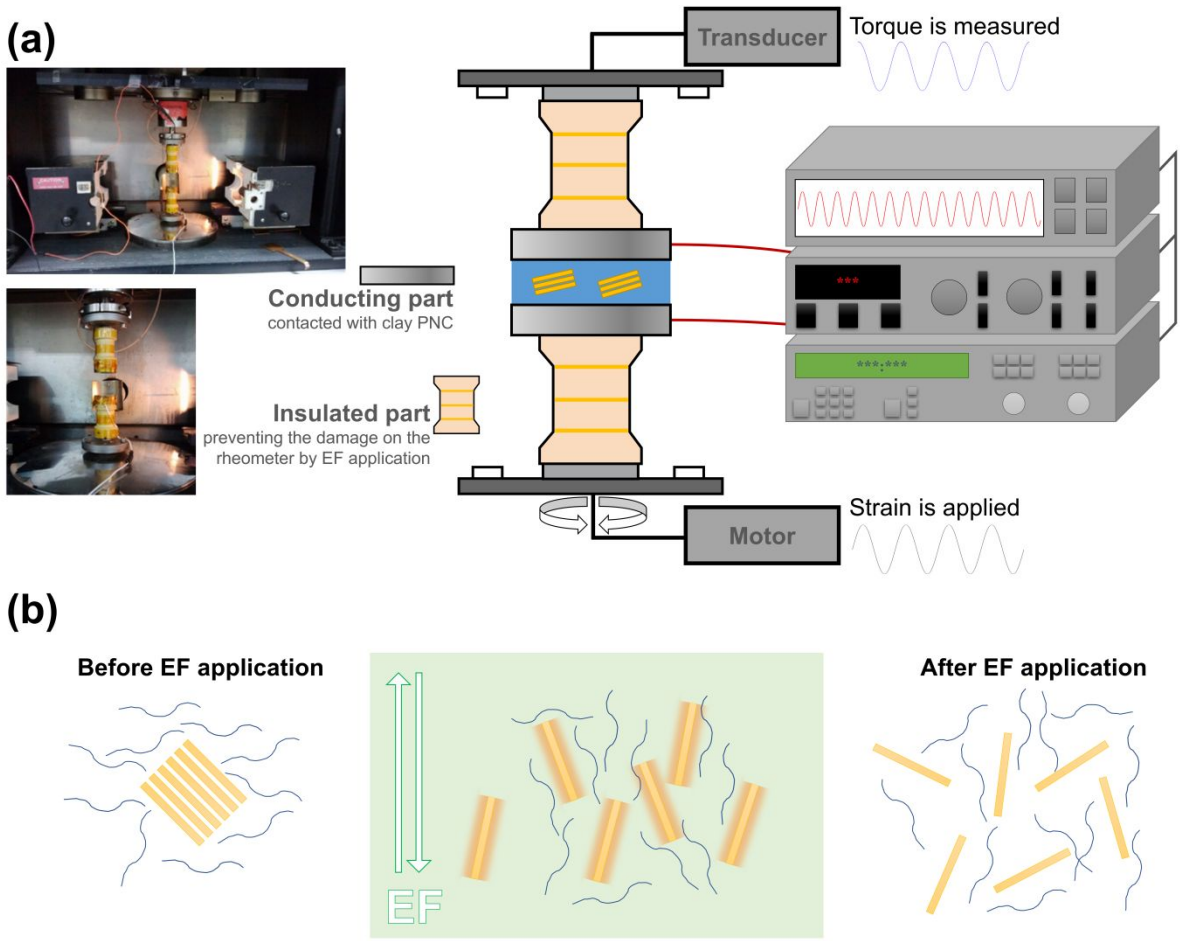

Figure 1. (a) Illustration of the electric field (EF) application setup. (b) Schematic of clay dispersion enhancement in the PP matrix under AC type EF application.

3. RESULTS AND DISCUSSION

3.1. Electric Field Application to PP/C20A PNCs. The time sweep test was conducted at a frequency of 1 rad/s and a strain amplitude of 0.03 within the linear viscoelastic (LVE) region. After 5 min, an AC EF was applied at 1 kV/mm strength and 60 Hz electric frequency for 3, 7, 10, 20, and 30 min. The time sweep test results are shown in Figure 2a. The *G*' and *G*" of PP/C20A5wt suddenly increased with time as soon as the EF was applied. The increases in *G*' and *G*" were mitigated over the EF-applied time of 7 min, reaching a plateau. *G*' showed more significant increases than *G*" for all EF-subjected PP/C20A5wt PNCs. According to Kim et al.,[16] the growth in *G*' closely correlates with the

morphological evolution, which is the exfoliation and intercalation of clay.[16] The detailed mechanism was revealed by dielectric relaxation analysis.[17,18] The bound ions on the clay surface dissociated under the AC EF, causing charge imbalance of van der Waals attractions and electrostatic repulsion between the adjacent stacked clay particles. Once the electrostatic repulsive force exceeds the attractive van der Waals force between the adjacent stacked clay particles, they repel each other and remain durable by penetrating the PP chains.

As soon as EF disappeared, aligned (forcedly restricted) clay particles would be randomly (Figure S2). Slight decrease in *G*' is explained by the disorder of individual particles (Figure S2). Under the electric field, clay particles aligned to the EF direction.[17,18] This makes the modulus decrease slightly. Regarding the amount of clay in the PP matrix under EF application, a higher clay content resulted in a more dramatic rise in *G*' (Figure 2b). This result can be explained by the total amount of clay exfoliation being limited by its original quantity when it reaches maximum efficiency. TEM observed the morphological evolution of PP/C20A PNCs to understand actual clay dispersion better.

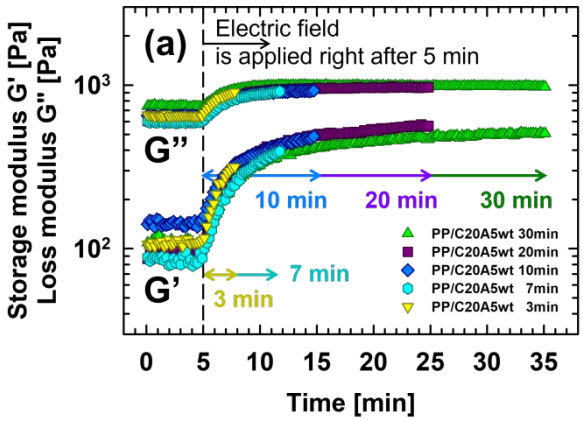

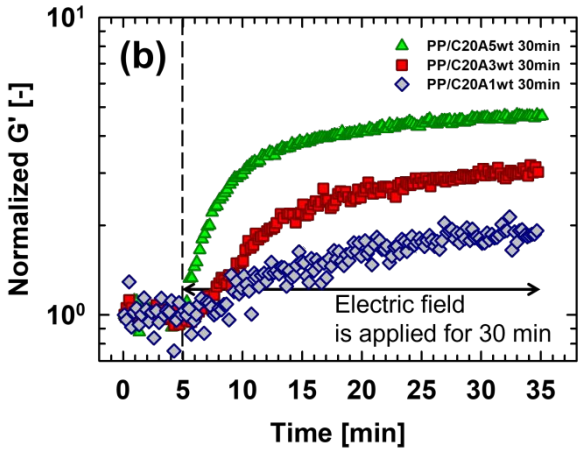

Figure 2. (a) Storage moduli (G') and loss moduli (G'') of PP/C20A5wt on varying EF-applied time as a function of time. After starting the measurement, the AC EF was applied for 3, 7, 10, 20, or 30 min at 5 min (300s) (arrows in the figure indicate EF-applied time). (b) Storage moduli normalized by the initial value of $G'(t \approx 0)$ for EF-applied time of 30 min at varying clay contents, 1, 3, and 5 wt%.

3.2. Morphological Observation for PP/C20A PNCs. Figure 3 presents TEM images of PP/C20A PNCs without EF application. Dispersed clay tactoids exhibited comparable dispersion states in the PP matrix without EF application (Figure 3). The agglomerates increased with increasing clay loading (1, 3, and 5 wt%) (Figure 3). On the other hand, it showed similar large agglomerate sizes regardless of the loading.

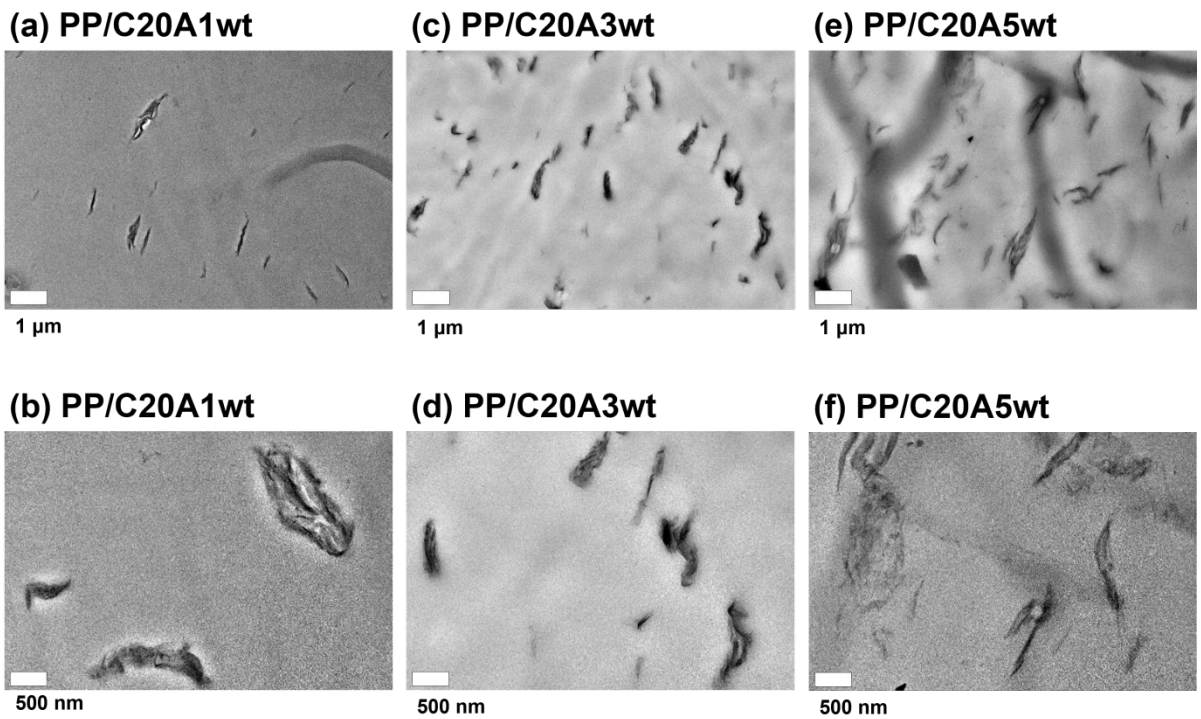

Figure 3. TEM images of PP/C20A PNCs without EF application: (a) and (b) PP/C20A1wt, (c) and (d) PP/C20A3wt, and (e) and (f) PP/C20A5wt. The scale bars are located at the left-bottom side of each image.

To check the effect of EF application, we present the morphology of EF-applied PP/C20A 5wt PNCs with increasing EF application times (3, 7, 10, 20, and 30 min) in Figure 4. The clay tactoids became smaller after only 3 minutes of EF application (Figure 4a) than without EF (Figure 3e,f). Clay was dispersed finely with longer EF application times (Figure 4b–d). Clay tactoids were finely dispersed by EF application for more than 20min in Figure 4e (intercalation state); they were dispersed almost individually at 30 min in Figure 4f (exfoliation state). In the initial study of EF-activated PNCs,[16] a similar system (comparable PP matrix and identical clay of equivalent loading) was subjected to 30min EF application and characterized by XRD and TEM. XRD revealed large-scale clay exfoliation by the disappearance of the d_{001} peak, supported by TEM. TEM can confirm clay dispersion. However, as TEM provides only qualitative information, we measured the rheological properties to obtain quantitative information about the clay dispersion.

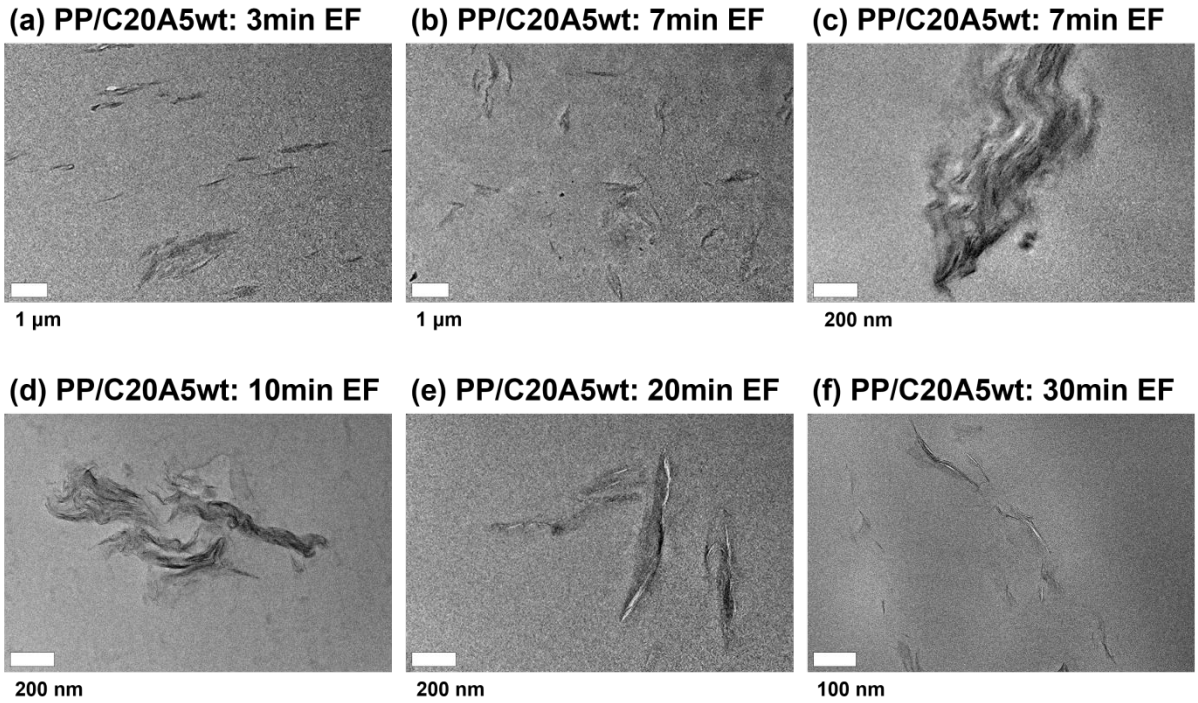

Figure 4. TEM images of PP/C20A5wt varying EF application time of (a) 3 min, (b) and (c) 7 min, (d) 10 min, (e) 20 min, and (f) 30 min. The scale bars are located at the left-bottom side of each image.

3.3. SAOS Test for PP/C20A PNCs. The SAOS test was conducted immediately after aborting the EF application at the various EF-applied times, 3, 7, 10, 20, and 30 min. This test is used widely to characterize PNCs to the filler dispersion quantitatively.[3–9] The SAOS results of PP/C20A5wt varying EF application time exhibited non-terminal behavior corresponding to the solid-like behavior induced by the filler loading and morphology evolution (Figure 5). The results for PP/C20A1wt and PP/C20A3wt are in Figure S3. It is observed in the low-frequency range prominently, reflected in SAOS parameters. Especially G' and $|\eta^*(\omega)|$ exhibited this solid-like behavior prominently. G' lose its scaling behavior in a lower frequency range as n decreases from 2 to near zero with better clay dispersity. $|\eta^*(\omega)|$ also reflected this solid-like behavior induced by solid particle loading.

The characteristic parameter n of SAOS was used to express the clay dispersion numerically.

The slope (n) of G' in the terminal region, ranging in 0.1–0.5 rad/s, was calculated using the power-law form equation:

$$G'(\omega) = k\omega^n \quad (1)$$

where k is a fitting coefficient, and n is the exponent and corresponds to the slope in the plot of log G' vs. log ω (Figure 5a). Table 1 lists the values from the equation fitting. PP usually showed the terminal behavior (n = 2) observed in homopolymers. n decreased somewhat with clay content up to 3 wt% (2 to 1.64) and reduced more with 5 wt% of clay loading (n = 1.10), achieved by mechanical mixing and filler loading. With EF application, n lowered dramatically from 0.71 with 3 min of EF application time to n = 0.27 with 30 min of EF application. Furthermore, reciprocals of n for PP/C20A PNCs were calculated in Table 1 and plotted in Figure S4 for better comparison.

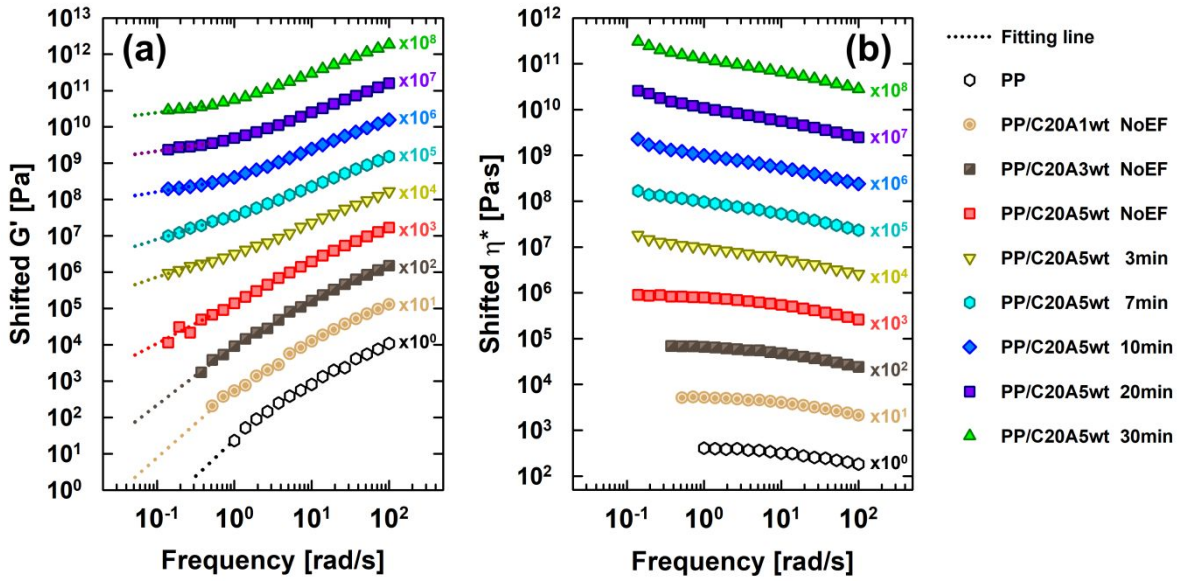

Figure 5. (a) Storage modulus and (b) complex viscosity of PP/C20A5wt with EF application time measured from 0.1 to 100 rad/s of the frequency at a strain amplitude of 0.03. $G'(\omega)$ and $|\eta^*(\omega)|$ of PP and PP/C20A with 1, 3, and 5 wt% of clay without the EF application were plotted together. The storage modulus is fitted by eq 1 in (a). The fitted results were added to each data as a dot-line. Data were shifted by the factors noted in the figures.

Table 1. Fitted Slopes (n) of G' in the Low-Frequency Range (0.1–0.5 rad/s) Using the Power-Law Equation (eq 1) for PP/C20A PNCs. And their reciprocals (1/n)

Samples	n [-] (eq 1)	$1/n$ [-]
PP	2	0.50
PP/C20A 1wt NoEF	1.89	0.53
PP/C20A 3wt NoEF	1.64	0.61
PP/C20A 5wt NoEF	1.10	0.91
PP/C20A 5wt 3min	0.71	1.41
PP/C20A 5wt 7min	0.68	1.47
PP/C20A 5wt 10min	0.35	2.86
PP/C20A 5wt 20min	0.31	3.23
PP/C20A 5wt 30min	0.27	3.70

Both n and $1/n$ reflected the clay dispersion enhancement and furnishing quantitative assessments. Primarily, $1/n$ provides more intuitive insight into the morphological evolution of clay in the PP matrix and presents identical bias with clay dispersity, i.e., $1/n$ rises when the dispersity improves. Kim et al.[8] studied clay dispersion in the PP/MAPP matrix using $1/n$ (instead of n) and compared it to clay dispersity. They observed the same trend for $1/n$ with clay dispersity, exhibiting higher values as their dispersion states are enhanced. In an additional application to a different PNC system, however, they failed to determine the dispersion state of the silica particles for PP/silica PNCs using the SAOS parameters.[8] Several studies reported the same issues.[9,12,13] These failures were usually noted for PNC containing spherical nanoparticles.

Recently, Hong et al.[21] used non-equilibrium molecular dynamics simulations to examine the viscoelastic property enhancements in a SAOS test for PNCs at varying nanosheet contents implemented using beads. They suggested that the enhancement of the moduli should be elucidated because the solid-like behaviors in PNCs at the terminal region could be attributed to the percolation network and the jamming of particles. According to their study, $G'(\omega)$ and $G''(\omega)$ increments were classified into three regimes according to the nanosheet contents, which are related to the Rouse dynamics, chain confinement, and percolation network. The polymer motion was hindered at lower nanosheet contents because of the interaction between the polymers and nanosheets, and the polymer chains commonly

followed the Rouse dynamics. As the nanosheet contents increased, the polymer chains were trapped between nanosheets, resulting in significant increases in G' and G''. At higher nanosheet contents, a percolation network of nanosheets was formed, which increased G' and G'' further. In addition, the effect of the polymer-nanosheet interaction was examined. An attractive interaction resulted in better nanosheet dispersion and increases in G' and G''. They offered more insight into the SAOS parameters of PNCs varying nanosheet filler contents and filler-polymer interaction to understand the moduli enhancement mechanisms. Although the SAOS parameters help lighten the morphological evolution regarding the filler dispersion in PNC, they are built too complicatedly from various contributions. Kim et al.[8] reported that the failure is because the SAOS parameters are affected complicatedly by interactions induced by fillers, matrices, and each other.

On the other hand, there is a lack of understanding of how the SAOS parameters are comprised. In previous studies characterizing filler dispersion in PNCs, Kim et al.[8,9] ascertained that the LAOS test is more valuable than the SAOS test. Morphological development (roughly increasing the interface area between polymer and filler) further increases LAOS parameters growth because the interfacial properties of heterogenous phases are reflected more in the LAOS parameters than SAOS parameters.[8,9,15] LAOS test is also worth conducting to characterize the clay dispersion in PP/C20A PNCs.

3.4. LAOS Test for PP/C20A PNCs. After the SAOS test, a strain amplitude sweep test was performed in strain amplitudes ranging from 0.01 to 5.0 at a fixed frequency of 1 rad/s to investigate the morphological development of PP/C20A PNCs. The complex modulus ($|G^*|$) and normalized $|G^*|$ ($\equiv |G^*|(\gamma_0)/|G^*|(\gamma_0 \approx 0)$) of PP/C20A PNCs and PP were plotted as a function of the strain amplitude in Figure 6 and Figure S5. PP/C20A PNCs without EF application showed increased modulus over the low strain amplitude range (Table S3) and earlier strain thinning behavior compared to neat PP on the clay loading (Figure 6a). It is well known as the Payne effect.[22] With increasing EF-applied time, i.e., as the clay dispersion improved, $|G^*|$ in the small strain amplitude range increased further (Table S3), and the critical strain amplitude (roughly onset point of strain thinning) moved to a lower strain amplitude than

PP/C20A5wt without EF application. As clay tactoids were dispersed finely with the EF-applied time, PP/C20A5wt PNCs under an EF exhibited a two-step strain thinning with a growing strain amplitude (Figure 6b). Kim et al.[8] observed similar behavior for highly clay-exfoliated PP/MAPP/clay PNCs. They attributed this to the individual clay particles being close to each other. As a result, clay particles form interconnected structures like the "House of Cards."[8,23] As clay particles are finely dispersed, the linear region is reduced by non-sinusoidal stress responses under large deformation. Further characterization was introduced to analyze the nonlinear responses of PP/C20A PNCs.

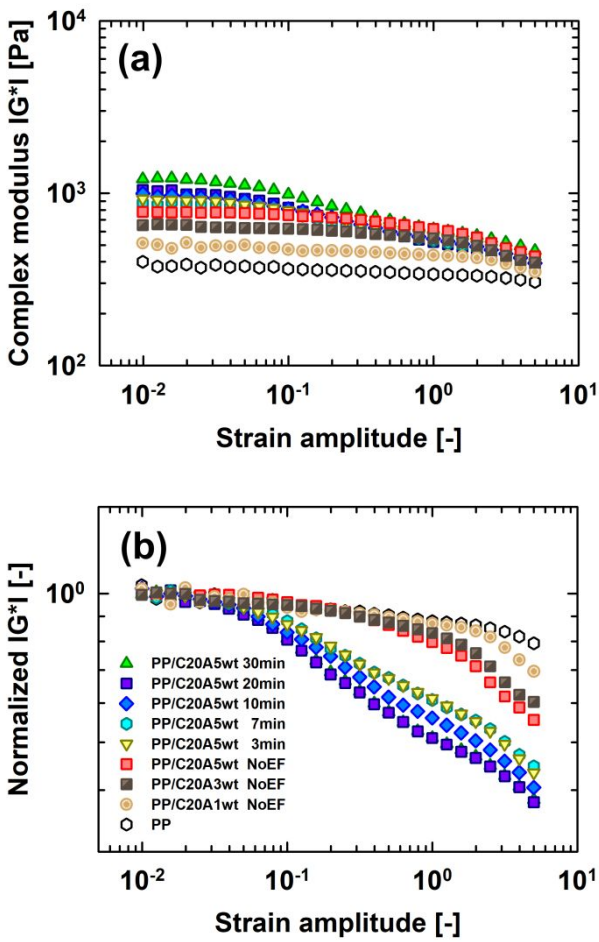

Figure 6. (a) Complex moduli $|G^*|$ and (b) the normalized $|G^*|$ ($= |G^*|(\gamma_0)/|G^*|(\gamma_0 \approx 0)$) of PP/C20A PNCs and PP as a function of the strain amplitude from 0.01 to 5.0 measured at a fixed frequency of 1 rad/s.

Analyzing these distorted stress responses is the primary key in LAOS test. There are several methods to characterize the LAOS test results, which are four LAOS types of responses in $G'(\gamma_0)$ and $G''(\gamma_0)$,[24,25] stress decomposition,[26,27] Chebyshev polynomials,[28] sequence of physical processes (SPP),[29,30] and FT-rheology[31–33]. FT-rheology has been introduced extensively because weak signals of higher harmonics can be quantified readily. The third harmonic intensity divided by the first,[31,32] i.e., $I_3/I_1 = I_{3/1}$, is one of the primary parameters utilized in FT-rheology.

The raw stress data of the strain sweep test for PP/C20A PNCs were analyzed using FT-rheology. The third harmonic intensity (I_3) in the FT spectrum is the most sensitive parameter to the stress curve distortion and emerges when the internal structure changes, i.e., in the nonlinear regime. The $I_{3/1}$ is the most representative parameter and is used widely to characterize polymeric materials.[15,19,34–48]

Owing to the junction between conducting and insulation parts of custom-built geometries, the noise in $I_{3/1}$ was more severe than that of the conventional geometries. The noise data at a small amplitude is not shown in Figure 7a and Figure S6. PP exhibited a quadratic relationship ($I_{3/1} \sim \gamma_0^2$) with the strain amplitude, and it has been observed generally for a polymer melt.[14,34–38,49] With clay loading, $I_{3/1}$ emerged in the lower strain amplitude with higher values, agreeing with the strain thinning behavior (shortening of the linear regime). For 5 wt% of clay loading, $I_{3/1}$ values were in the range between 4×10^{-3} and 2.5×10^{-2} of the grey area in Figure 7a.

Furthermore, $I_{3/1}$ emerged at a lower strain amplitude range with increasing EF-applied time but remained in the grey area ($4\times10^{-3} \sim 2.5\times10^{-2}$ in Figure 7a). With increasing clay content and EF application duration, the $I_{3/1}$ values of PP/C20A PNCs demonstrated their morphological development by appearing at lower strain amplitudes and increasing values. An additional nonlinear parameter was introduced to quantify the nonlinear behavior of PP/C20A PNCs and express the results more intuitively.

$I_{3/1}$ depends quadratically on the medium amplitude oscillatory shear (MAOS) region between the SAOS and LAOS regions. It is a well-known relationship for polymer solutions[50–52] and melts[14,34–38,49], PNCs,[8,9,15,19,41,53] and polymer blends[42–48,54]. With the quadric relationship of $I_{3/1}$ to strain amplitude, Hyun and Wilhelm[14] proposed nonlinear parameters:

$$Q(\gamma_0)\ [\equiv I_{3/1}/\gamma_0^2] \text{ and } Q_0\ [\lim_{\gamma_0 \to 0} Q(\gamma_0) \equiv Q_0\ ] \quad (2)$$

Nonlinear parameters were plotted in Figure 7b and Figure S7 and calculated in Table S3. The Q parameter of neat PP exhibited the lowest value due to the morphological homogeneity. From the clay loading, the Q of PP/C20A PNCs in the absence of an EF emerged at lower strain amplitude with a more considerable value (red-dot arrow in Figure 7b). In addition, Q of PP/C20A5wt with EF application developed at a lower strain amplitude with the highest value (green-dash arrow in Figure 7b). $I_{3/1}$ also showed linear regime shortening for clay dispersion enhancement but exhibited a similar level (4×10^{-3}~2.5×10^{-2}) in the grey area in Figure 7a. With clay dispersion enhancement, the internal structure of PP/C20A became complicated and easy to break down by smaller deformation, resulting in an increase in $I_{3/1}$ value and a decrease in critical strain. On the other hand, $I_{3/1}$ exhibited a limited value (approximately 2.5×10^{-2}) even with further dispersion enhancement.

On the other hand, the Q parameter can involve this linear regime shortening and intensity increment together by its definition ($Q(\gamma_0) \equiv I_{3/1}/\gamma_0^2$), and the Q_0 parameter can quantify these together.

The Q_0 parameters were calculated using the model suggested by Lim et al.[15]:

$$Q = Q_0(1 + (C_1\gamma_0)^{C_2})^{(C_3-1)/C_2} \quad (3)$$

where C_1, C_2, and C_3 are fitting parameters. The clay dispersion was enhanced with increasing clay contents and EF application duration, and the $I_{3/1}$ values increased and spread to the lower strain amplitude region. As a result, the Q_0 parameter was amplified by the $I_{3/1}$ increment and the onset at lower γ_0. The clay loading to PP without EF application increased $|G^*|$ in Figure 6a and Q_0 in Figure 7b to some extent (See Table S4: Q_0(PP/C20A5wt)/Q_0(PP) = 22.8 and $|G^*|$(PP/C20A5wt)/$|G^*|$(PP) = 2.05). Q_0 exhibited significant increments with increasing EF-applied time for PP/C20A5wt (Figure 7b). Nonlinear parameter Q_0 demonstrated a more prominent response to clay dispersion enhancement by EF than $|G^*|$. The same tendency was observed in previous studies.[8,9,15]

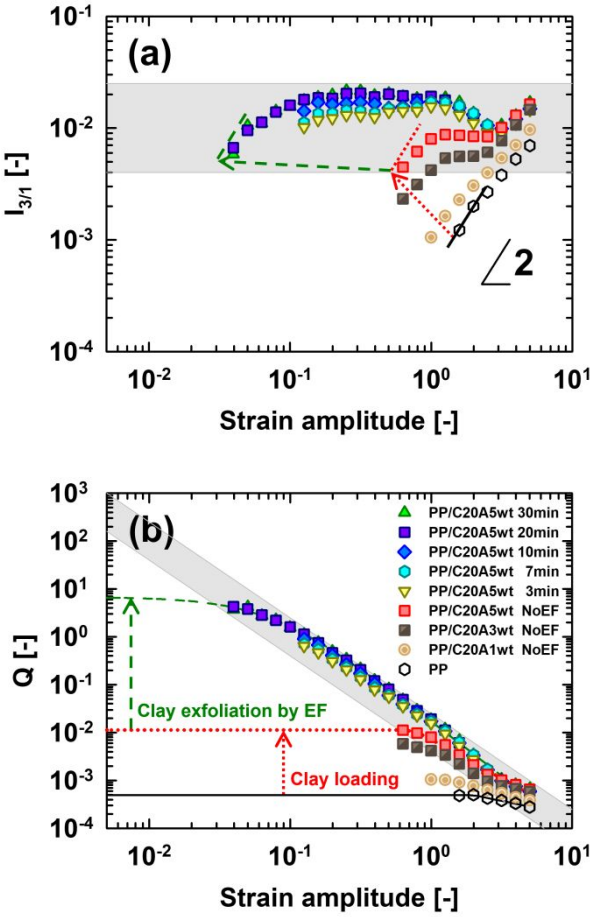

Figure 7. (a) Nonlinearities $I_{3/1}$ and (b) Q of PP/C20A PNCs and PP as a function of strain amplitude (noise data in small strain amplitudes were deleted). The grey area in the figure of $I_{3/1}$ was placed in $I_{3/1}$ values ranging from 0.004 to 0.025. The grey area in the figure of Q corresponds to that of $I_{3/1}$.

3.5. Quantification of Clay Dispersion in PP/C20A PNCs. Q_0 and $|G^*|$ normalized by each PP data were calculated to compare it quantitively (Table S4 and Figure S8). The increasing Q_0 breadth was more prominent than in $|G^*|$ regarding clay-dispersion enhancement (Table S4 and Figure S8). These results concurred with the previous studies.[8,9,15] G' and $|G^*|$ of both tests showed relevant higher values at higher dispersion states. Both $|G^*|$ and Q_0 parameters reflected clay dispersion enhancements well for PP/C20A PNCs. On the other hand, the change in Q_0 showed more distinct variations for clay dispersion enhancement, e.g., Q_0(PP/C20A5wt 30min)/Q_0(PP) = 13,540 and $|G^*|$(PP/C20A5wt 30min)/$|G^*|$(PP) =

3.24 (Table S4).

Once the polymer matrix is filled with fillers, the modulus increases significantly in the small strain amplitude range (LVE regime). Simultaneously, the onset strain amplitude of the nonlinear regime decreases with more pronounced strain thinning under increasing oscillatory deformation, known as the Payne effect. The decrease in modulus with increasing strain amplitude was attributed to the breakdown of the physical filler-filler network structure. These nonlinear behaviors increased with increasing filler content and more vital interactions between fillers. Similarly, Lim et al.[15] analyzed the PNCs by conducting the strain sweep test analyzed with FT-rheology and suggested a nonlinear parameter, nonlinear-linear viscoelastic ratio (NLR), to quantify the degree of dispersion for PNCs.

$$NLR = \frac{Q_0(\varphi) / Q_0(0)}{|G^*(\varphi)| / |G^*(0)|} \tag{4}$$

where $|G^*|$ is the complex modulus measured in the SAOS region, φ is filler content, and 0 means the base polymer without a filler, here PP. The NLR parameter is defined as the ratio of nonlinear parameter increase with filler contents to that of the linear parameter. Lim et al.[15] characterized polycaprolactone nanocomposites incorporating the inorganic filler (multi-walled carbon nanotubes, organo-clay, or precipitated calcium carbonate), using linear (G' and $|G^*|$) and nonlinear parameters from FT-rheology (NLR and Q_0). According to them, the nonlinear properties were more sensitive to morphological developments by the filler contents than those of linear (SAOS parameters). Kim et al.[8,9] used NLR to assess the filler dispersion in PNCs containing clay or silica particles and observed that NLR showed agreement with their morphology. For PNCs, including silica, NLR and Q_0 coincided with their morphological evolution, whereas SAOS parameters failed.

The NLR parameters for PP/C20A PNCs were calculated (Table S4) and plotted in Figure 8. Obtaining high dispersion quality of clay in the PP matrix was difficult because of the lack of affinity between the two components. Clay tactoids sizes in TEM images of PP/C20A with 1, 3, and 5 wt% of clay were similar, and the tactoids were located just more frequently with clay contents (Figure 3). The NLR parameters increased monotonically with increasing clay content (Bottom line in Figure 8). The

clay tactoids were dispersed finely using EF application to PP/C20A PNCs (Figure 4). The interface between clay and PP tremendously increased by clay exfoliation owing to the high aspect ratio of a single clay particle (Figure 4). This was reflected in the NLR parameters by increasing EF-applied time and clay contents (Upper line in Figure 8). In addition, the trend of Q_0 was strongly reflected in the NLR because the growth in normalized Q_0 value is more prominent than normalized $|G^*|$ (see Table S4, Q_0(PP/C20A5wt 30min)/Q_0(PP) = 13,540 and $|G^*|$(PP/C20A5wt 30min)/$|G^*|$(PP) = 3.24).

The NLR parameters concerning filler dispersion in PNC and its relationship were examined using FT-rheology measurements for PP/C20A PNCs. The clay-polymer interface increased enormously because of the high aspect ratio of the clay particles. With the EF application time and clay amount, stacked clay agglomerates dispersed into a few clay platelets (see Figure 3 and Figure 4). Linear rheological measurements exhibited the same results as TEM observation. The lower slope n and higher $1/n$ of G' in the low-frequency range appeared in higher clay dispersion states (higher loading and longer EF application time). The NLR parameters also corresponded to the same order with designed PP/C20A PNCs, expressing higher values at highly dispersed clay in PP. The changes in nonlinear parameters would be strongly matched with the interfacial area between the matrix and filler as they were designed by EF application and clay contents.

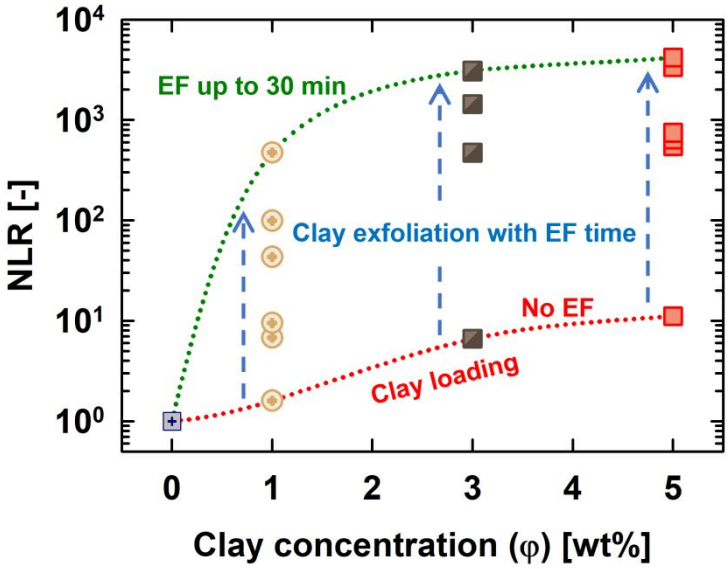

Figure 8. NLR values for PP/C20A PNCs as a function of C20A concentration. Effects of C20A loading (red-dot lower line for No EF) and EF application duration (blue-vertical arrows and green-dot upper line up to 30 min EF) on PP/C20A PNCs corresponding to each morphological development as a higher value at enhanced dispersity. The data used in the figure correspond with Table S4.

4. CONCLUSIONS

This study investigated rheological parameters from SAOS and LAOS tests for characterizing clay dispersion in polypropylene (PP) of polymer nanocomposites (PNCs). PP/clay PNC system was introduced to study the changes in the rheological properties of SAOS and LAOS on morphological evolution because clay affects the rheological properties sensitively by changing its internal structure variation. PP/C20A PNCs were subjected to the electric field (EF) application (AC type 1.0kV/mm and 60Hz) on the melt state on a rheometer to fabricate the clay dispersion in the PP matrix. The EF application duration and the clay content manipulated clay dispersity. The clay dispersion was regarded as the interface area (intercalation and exfoliation) between clay and PP, achieved by mechanical mixing and EF application. The interface varied considerably on the difference in clay dispersion because of the large aspect ratio.

SAOS parameters showed monotonic increases by the clay loading and EF application duration. In contrast, LAOS parameters showed more extreme responses with the clay content and EF application time to PP/C20A PNCs. When the concentration of clay increased without EF application (φ = 1,3, and 5wt%), $|G^*|(\varphi)/|G^*|(PP)$ increased from 1 to 2.05. $I_{3/1}$ of PP/C20A PNCs showed higher values and emerged at lower strain amplitudes than PP. $I_{3/1}$ of PP/C20A with EF application emerged at a lower strain amplitude range than PP/C20A without EF application but showed a similar level (0.004 to 0.025).

The Q parameter could consider the higher values in $I_{3/1}$ and linear regime shortening (= critical strain amplitude decrement) by its definition ($Q \equiv I_{3/1}/\gamma_0^2$). The Q parameters displayed higher values at a lower strain amplitude strongly with increasing clay contents and EF application duration. Q_0 parameters were calculated to quantify these nonlinear behaviors and showed the same trend of the SAOS test; distinct higher values for higher dispersion states.

Q_0(PP/C20A5wt)/Q_0(PP) increased from 1 to 22.8. In 5wt% clay PNC, EF was applied in increments of 3,7,10,20, and 30min. With increasing EF application time up to 30min, $|G^*|$(PP/C20A5wt 30min)/$|G^*|$(PP) increased from 1 to 3.24, while Q_0(PP/C20A5wt 30min)/Q_0(PP) increased significantly from 1 to 13,540. Nonlinear parameters Q and Q_0 exhibited increased extremely with clay dispersion enhancement. It is owing to the definition of Q parameter ($Q(\gamma_0) \equiv I_{3/1}/\gamma_0^2$). NLR was also used to quantify the degree of dispersion for PP/C20A PNCs compatibilized by EF application. The NLR parameters of PP/C20A PNCs increased slightly with increasing clay contents and soared vigorously with the EF application duration.

Though both SAOS and LAOS parameters demonstrated clay dispersion in PP/C20A PNCs, the LAOS parameters showed more variation for clay dispersion than SAOS parameters, resulting in distinct characterization for filler dispersion. As the clay dispersion from the tactoids to exfoliation states, $Q_0(\varphi)/Q_0(PP)$ increased significantly from 1 to 13,540, while $|G^*|(\varphi)/|G^*|(PP)$ increased from 1 to 3.24. Checking both methods is worthwhile; however, sensitive variations in LAOS for filler dispersion provide clearer insight between the comparable PNCs than in SAOS.

■ ASSOCIATED CONTENT

Supporting Information

The Supporting Information is available free of charge at https://pubs.acs.org/doi/-.

Material information (Table S1), specimen formulation (Table S2), rheological parameters values utilized for figures in the manuscript (Table S3 and S4), rheological measurements description (Figure S1), storage modulus responses on the time with/without electric field application (Figure S2), and rheological data for 1 and 3 wt% PP/C20A PNCs (Figure S3~S8)

■ AUTHOR INFORMATION

Corresponding Author

Kyu Hyun – *School of Chemical Engineering, Pusan National University, Busan, 46241, Republic of Korea;* orcid.org/0000-0001-5129-5169; Email: kyuhyun@pusan.ac.kr

Authors

Mingeun Kim – *School of Chemical Engineering, Pusan National University, Busan, 46241, Republic of Korea; Chemical Materials Solutions Center, Korea Research Institute of Chemical Technology (KRICT), Daejeon 34114, Republic of Korea;* orcid.org/0000-0001-5325-3245

Min Chan Kim – *School of Chemical Engineering, Pusan National University, Busan, 46241, Republic of Korea;* orcid.org/0009-0003-9130-1473

Reza Salehiyan – *School of Computing, Engineering and Built Environment, Edinburgh Napier University, Edinburgh, EH10 5DT, United Kingdom;* orcid.org/0000-0001-5345-5162

Jin Suk Myung – *Chemical Materials Solutions Center, Korea Research Institute of Chemical Technology (KRICT), Daejeon, 34114, Republic of Korea;* orcid.org/0000-0003-2111-1917

Woo Jin Choi – *Chemical Materials Solutions Center, Korea Research Institute of Chemical Technology (KRICT), Daejeon, 34114, Republic of Korea;* orcid.org/0000-0003-1173-2365

Notes

The authors declare no competing financial interest.

■ ACKNOWLEDGMENTS

This work was supported by a National Research Foundation of Korea (NRF) grant funded by the Korean government (MSIT) (2021R1I1A3054572 and 2021M3H4A1A03041403).

■ REFERENCES

(1) Okada, A.; Kawasumi, M.; Usuki, A.; Kojima, Y.; Kurauchi, T.; Kamigaito, O. Nylon 6–Clay Hybrid. *MRS Online Proc. Libr.* **1989**, *171*, 45–50. https://doi.org/10.1557/PROC-171-45.

(2) Sinha Ray, S.; Okamoto, M. Polymer/Layered Silicate Nanocomposites: A Review from Preparation to Processing. *Prog. Polym. Sci.* **2003**, *28*, 1539–1641. https://doi.org/10.1016/j.progpolymsci.2003.08.002.

(3) Krishnamoorti, R.; Yurekli, K. Rheology of Polymer Layered Silicate Nanocomposites. *Curr. Opin. Colloid Interface Sci.* **2001**, *6*, 464–470. https://doi.org/10.1016/S1359-0294(01)00121-2.

(4) Ren, J.; Krishnamoorti, R. Nonlinear Viscoelastic Properties of Layered-Silicate-Based Intercalated Nanocomposites. *Macromolecules* **2003**, *36*, 4443–4451. https://doi.org/10.1021/ma020412n.

(5) Gu, S. Y.; Ren, J.; Wang, Q. F. Rheology of Poly(Propylene)/Clay Nanocomposites. *J. Appl. Polym. Sci.* **2004**, *91*, 2427–2434. https://doi.org/10.1002/app.13403.

(6) Vermant, J.; Ceccia, S.; Dolgovskij, M. K.; Maffettone, P. L.; Macosko, C. W. Quantifying Dispersion of Layered Nanocomposites via Melt Rheology. *J. Rheol.* **2007**, *51*, 429–450. https://doi.org/10.1122/1.2516399.

(7) Lertwimolnun, W.; Vergnes, B. Influence of Compatibilizer and Processing Conditions on the Dispersion of Nanoclay in a Polypropylene Matrix. *Polymer* **2005**, *46*, 3462–3471. https://doi.org/10.1016/j.polymer.2005.02.018.

(8) Kim, M.; Song, H. Y.; Choi, W. J.; Hyun, K. Evaluation of the Degree of Dispersion of Polymer Nanocomposites (PNCs) Using Nonlinear Rheological Properties by FT-Rheology. *Macromolecules* **2019**, *52*, 8604–8616. https://doi.org/10.1021/acs.macromol.9b01302.

(9) Kim, M.; Hyun, K. Characterization of Polyethylene/Silica Nanocomposites Using Different Rheological Analyses. *Korea-Aust. Rheol. J.* **2021**, *33*, 25–36. https://doi.org/10.1007/s13367-021-0003-3.

(10) Jang, K. S.; Yeom, H. Y.; Park, J. W.; Lee, S. H.; Lee, S. J. Morphology, Electrical Conductivity, and Rheology of Latex-Based Polymer/Nanocarbon Nanocomposites. *Korea-Aust. Rheol. J.* **2021**, *33*, 357–366. https://doi.org/10.1007/s13367-021-0028-7.

(11) Kim, H. J.; Jeong, J. H.; Choi, Y. H.; Eom, Y. Review on Cellulose Nanocrystal-Reinforced Polymer Nanocomposites: Processing, Properties, and Rheology. *Korea-Aust. Rheol. J.* **2021**, *33*, 165–185. https://doi.org/10.1007/s13367-021-0015-z.

(12) Zhao, D.; Ge, S.; Senses, E.; Akcora, P.; Jestin, J.; Kumar, S. K. Role of Filler Shape and Connectivity on the Viscoelastic Behavior in Polymer Nanocomposites. *Macromolecules* **2015**, *48*, 5433–5438. https://doi.org/10.1021/acs.macromol.5b00962.

(13) Senses, E.; Jiao, Y.; Akcora, P. Modulating Interfacial Attraction of Polymer-Grafted Nanoparticles in Melts under Shear. *Soft Matter* **2014**, *10*, 4464–4470. https://doi.org/10.1039/C4SM00460D.

(14) Hyun, K.; Wilhelm, M. Establishing a New Mechanical Nonlinear Coefficient *Q* from FT-Rheology: First Investigation of Entangled Linear and Comb Polymer Model Systems. *Macromolecules* **2009**, *42*, 411–422. https://doi.org/10.1021/ma8017266.

(15) Lim, H. T.; Ahn, K. H.; Hong, J. S.; Hyun, K. Nonlinear Viscoelasticity of Polymer Nanocomposites under Large Amplitude Oscillatory Shear Flow. *J. Rheol.* **2013**, *57*, 767–789. https://doi.org/10.1122/1.4795748.

(16) Kim, D. H.; Park, J. U.; Ahn, K. H.; Lee, S. J. Electrically Activated Poly(Propylene)/Clay Nanocomposites. *Macromol. Rapid Commun.* **2003**, *24*, 388–391. https://doi.org/10.1002/marc.200390055.

(17) Park, J. U.; Choi, Y. S.; Cho, K. S.; Kim, D. H.; Ahn, K. H.; Lee, S. J. Time–Electric Field Superposition in Electrically Activated Polypropylene/Layered Silicate Nanocomposites. *Polymer* **2006**, *47*, 5145–5153. https://doi.org/10.1016/j.polymer.2006.05.018.

(18) Kim, D. H.; Cho, K. S.; Mitsumata, T.; Ahn, K. H.; Lee, S. J. Microstructural Evolution of Electrically Activated Polypropylene/Layered Silicate Nanocomposites Investigated by in Situ Synchrotron Wide-Angle X-Ray Scattering and Dielectric Relaxation Analysis. *Polymer* **2006**, *47*, 5938–5945. https://doi.org/10.1016/j.polymer.2006.06.029.

(19) Hyun, K.; Lim, H. T.; Ahn, K. H. Nonlinear Response of Polypropylene (PP)/Clay Nanocomposites under Dynamic Oscillatory Shear Flow. *Korea-Aust. Rheol. J.* **2012**, *24*, 113–120. https://doi.org/10.1007/s13367-012-0013-2.

(20) Ock, H. G.; Ahn, K. H.; Lee, S. J. Effect of Electric Field on Polymer/Clay Nanocomposites Depending on the Affinities between the Polymer and Clay. *J. Appl. Polym. Sci.* **2016**, *133*, 43582. https://doi.org/10.1002/app.43582.

(21) Hong, W.; Lin, J.; Tian, X.; Wang, L. Viscoelasticity of Nanosheet-Filled Polymer Composites: Three Regimes in the Enhancement of Moduli. *J. Phys. Chem. B* **2020**, *124*, 6437–6447. https://doi.org/10.1021/acs.jpcb.0c04235.

(22) Payne, A. R. The Dynamic Properties of Carbon Black-Loaded Natural Rubber Vulcanizates. Part I. *J. Appl. Polym. Sci.* **1962**, *6*, 57–63. https://doi.org/10.1002/app.1962.070061906.

(23) Okamoto, M.; Nam, P. H.; Maiti, P.; Kotaka, T.; Hasegawa, N.; Usuki, A. A House of Cards Structure in Polypropylene/Clay Nanocomposites under Elongational Flow. *Nano Lett.* **2001**, *1*, 295–298. https://doi.org/10.1021/nl0100163.

(24) Hyun, K.; Kim, S. H.; Ahn, K. H.; Lee, S. J. Large Amplitude Oscillatory Shear as a Way to Classify the Complex Fluids. *J. Non-Newton. Fluid Mech.* **2002**, *107*, 51–65. https://doi.org/10.1016/S0377-0257(02)00141-6.

(25) Hyun, K.; Wilhelm, M.; Klein, C. O.; Cho, K. S.; Nam, J. G.; Ahn, K. H.; Lee, S. J.; Ewoldt, R. H.; McKinley, G. H. A Review of Nonlinear Oscillatory Shear Tests: Analysis and Application of Large Amplitude Oscillatory Shear (LAOS). *Prog. Polym. Sci.* **2011**, *36*, 1697–1753.

https://doi.org/10.1016/j.progpolymsci.2011.02.002.

(26) Cho, K. S.; Hyun, K.; Ahn, K. H.; Lee, S. J. A Geometrical Interpretation of Large Amplitude Oscillatory Shear Response. *J. Rheol.* **2005**, *49*, 747–758. https://doi.org/10.1122/1.1895801.

(27) Cho, K. S.; Bae, J. E. Geometric Insights on Viscoelasticity: Symmetry, Scaling and Superposition of Viscoelastic Functions. *Korea-Aust. Rheol. J.* **2011**, *23*, 49–58. https://doi.org/10.1007/s13367-011-0007-5.

(28) Ewoldt, R. H.; Hosoi, A. E.; McKinley, G. H. New Measures for Characterizing Nonlinear Viscoelasticity in Large Amplitude Oscillatory Shear. *J. Rheol.* **2008**, *52*, 1427–1458. https://doi.org/10.1122/1.2970095.

(29) Rogers, S. A.; Erwin, B. M.; Vlassopoulos, D.; Cloitre, M. A Sequence of Physical Processes Determined and Quantified in LAOS: Application to a Yield Stress Fluid. *J. Rheol.* **2011**, *55*, 435–458. https://doi.org/10.1122/1.3544591.

(30) Park, J. D.; Rogers, S. A. Rheological Manifestation of Microstructural Change of Colloidal Gel under Oscillatory Shear Flow. *Phys. Fluids* **2020**, *32*, 063102. https://doi.org/10.1063/5.0006792.

(31) Wilhelm, M. Fourier-Transform Rheology. *Macromol. Mater. Eng.* **2002**, *287*, 83–105. https://doi.org/10.1002/1439-2054(20020201)287:2<83::AID-MAME83>3.0.CO;2-B.

(32) Wilhelm, M.; Reinheimer, P.; Ortseifer, M. High Sensitivity Fourier-Transform Rheology. *Rheol. Acta* **1999**, *38*, 349–356. https://doi.org/10.1007/s003970050185.

(33) Wilhelm, M.; Maring, D.; Spiess, H. W. Fourier-Transform Rheology. *Rheol. Acta* **1998**, *37*, 399–405. https://doi.org/10.1007/s003970050126.

(34) Schlatter, G.; Fleury, G.; Muller, R. Fourier Transform Rheology of Branched Polyethylene: Experiments and Models for Assessing the Macromolecular Architecture. *Macromolecules* **2005**, *38*, 6492–6503. https://doi.org/10.1021/ma0505530.

(35) Wagner, M. H.; Rolón-Garrido, V. H.; Hyun, K.; Wilhelm, M. Analysis of Medium Amplitude Oscillatory Shear Data of Entangled Linear and Model Comb Polymers. *J. Rheol.* **2011**, *55*, 495–516. https://doi.org/10.1122/1.3553031.

(36) Kempf, M.; Ahirwal, D.; Cziep, M.; Wilhelm, M. Synthesis and Linear and Nonlinear Melt

Rheology of Well-Defined Comb Architectures of PS and PpMS with a Low and Controlled Degree of Long-Chain Branching. *Macromolecules* **2013**, *46* (12), 4978–4994. https://doi.org/10.1021/ma302033g.

(37) Hoyle, D. M.; Auhl, D.; Harlen, O. G.; Barroso, V. C.; Wilhelm, M.; McLeish, T. C. B. Large Amplitude Oscillatory Shear and Fourier Transform Rheology Analysis of Branched Polymer Melts. *J. Rheol.* **2014**, *58* (4), 969–997. https://doi.org/10.1122/1.4881467.

(38) Cziep, M. A.; Abbasi, M.; Heck, M.; Arens, L.; Wilhelm, M. Effect of Molecular Weight, Polydispersity, and Monomer of Linear Homopolymer Melts on the Intrinsic Mechanical Nonlinearity ${}^{3}Q_0(\omega)$ in MAOS. *Macromolecules* **2016**, *49*, 3566–3579. https://doi.org/10.1021/acs.macromol.5b02706.

(39) Reinheimer, K.; Grosso, M.; Wilhelm, M. Fourier Transform Rheology as a Universal Non-Linear Mechanical Characterization of Droplet Size and Interfacial Tension of Dilute Monodisperse Emulsions. *J. Colloid Interface Sci.* **2011**, *360*, 818–825. https://doi.org/10.1016/j.jcis.2011.05.002.

(40) Reinheimer, K.; Grosso, M.; Hetzel, F.; Kübel, J.; Wilhelm, M. Fourier Transform Rheology as an Innovative Morphological Characterization Technique for the Emulsion Volume Average Radius and Its Distribution. *J. Colloid Interface Sci.* **2012**, *380*, 201–212. https://doi.org/10.1016/j.jcis.2012.03.079.

(41) Schwab, L.; Hojdis, N.; Lacayo, J.; Wilhelm, M. Fourier-Transform Rheology of Unvulcanized, Carbon Black Filled Styrene Butadiene Rubber. *Macromol. Mater. Eng.* **2016**, *301*, 457–468. https://doi.org/10.1002/mame.201500356.

(42) Carotenuto, C.; Grosso, M.; Maffettone, P. L. Fourier Transform Rheology of Dilute Immiscible Polymer Blends: A Novel Procedure To Probe Blend Morphology. *Macromolecules* **2008**, *41*, 4492–4500. https://doi.org/10.1021/ma800540n.

(43) Salehiyan, R.; Yoo, Y.; Choi, W. J.; Hyun, K. Characterization of Morphologies of Compatibilized Polypropylene/Polystyrene Blends with Nanoparticles via Nonlinear Rheological Properties from FT-Rheology. *Macromolecules* **2014**, *47*, 4066–4076. https://doi.org/10.1021/ma500700e.

(44) Salehiyan, R.; Song, H. Y.; Choi, W. J.; Hyun, K. Characterization of Effects of Silica Nanoparticles on (80/20) PP/PS Blends via Nonlinear Rheological Properties from Fourier Transform Rheology. *Macromolecules* **2015**, *48*, 4669–4679. https://doi.org/10.1021/acs.macromol.5b00679.

(45) Salehiyan, R.; Song, H. Y.; Kim, M.; Choi, W. J.; Hyun, K. Morphological Evaluation of PP/PS Blends Filled with Different Types of Clays by Nonlinear Rheological Analysis. *Macromolecules* **2016**, *49*, 3148–3160. https://doi.org/10.1021/acs.macromol.6b00268.

(46) Lee, C. J.; Salehiyan, R.; Ham, D. S.; Cho, S. K.; Lee, S. J.; Kim, K. J.; Yoo, Y.; Hyun, K.; Lee, J. H.; Choi, W. J. Influence of Carbon Nanotubes Localization and Transfer on Electrical Conductivity in PA66/(PS/PPE)/CNTs Nanocomposites. *Polymer* **2016**, *84*, 198–208. https://doi.org/10.1016/j.polymer.2015.12.055.

(47) Ock, H. G.; Ahn, K. H.; Lee, S. J.; Hyun, K. Characterization of Compatibilizing Effect of Organoclay in Poly(Lactic Acid) and Natural Rubber Blends by FT-Rheology. *Macromolecules* **2016**, *49*, 2832–2842. https://doi.org/10.1021/acs.macromol.5b02157.

(48) Lee, S.; Kim, M.; Song, H. Y.; Hyun, K. Characterization of the Effect of Clay on Morphological Evaluations of PLA/Biodegradable Polymer Blends by FT-Rheology. *Macromolecules* **2019**, *52*, 7904–7919. https://doi.org/10.1021/acs.macromol.9b00800.

(49) Song, H. Y.; Nnyigide, O. S.; Salehiyan, R.; Hyun, K. Investigation of Nonlinear Rheological Behavior of Linear and 3-Arm Star 1,4-Cis-Polyisoprene (PI) under Medium Amplitude Oscillatory Shear (MAOS) Flow via FT-Rheology. *Polymer* **2016**, *104*, 268–278. https://doi.org/10.1016/j.polymer.2016.04.052.

(50) Song, H. Y.; Hyun, K. Decomposition of Q_0 from FT-Rheology into Elastic and Viscous Parts: Intrinsic-Nonlinear Master Curves for Polymer Solutions. *J. Rheol.* **2018**, *62*, 919–939. https://doi.org/10.1122/1.5024720.

(51) Song, H. Y.; Hyun, K. First-Harmonic Intrinsic Nonlinearity of Model Polymer Solutions in Medium Amplitude Oscillatory Shear (MAOS). *Korea-Aust. Rheol. J.* **2019**, *31*, 1–13. https://doi.org/10.1007/s13367-019-0001-x.

(52) Song, H. Y.; Park, S. J.; Hyun, K. Characterization of Dilution Effect of Semidilute Polymer Solution on Intrinsic Nonlinearity Q_0 via FT Rheology. *Macromolecules* **2017**, *50*, 6238–6254. https://doi.org/10.1021/acs.macromol.7b00119.

(53) Hassanabadi, H. M.; Wilhelm, M.; Rodrigue, D. A Rheological Criterion to Determine the Percolation Threshold in Polymer Nano-Composites. *Rheol. Acta* **2014**, *53*, 869–882. https://doi.org/10.1007/s00397-014-0804-0.

(54) Sangroniz, L.; Palacios, J. K.; Fernández, M.; Eguiazabal, J. I.; Santamaria, A.; Müller, A. J. Linear and Non-Linear Rheological Behavior of Polypropylene/Polyamide Blends Modified with a Compatibilizer Agent and Nanosilica and Its Relationship with the Morphology. *Eur. Polym. J.* **2016**, *83*, 10–21. https://doi.org/10.1016/j.eurpolymj.2016.07.026.

For Table of Contents use only

Clay Dispersion Assessment via FT-Rheology for Polypropylene/Clay Nanocomposites Fabricated by Electric Field

Mingeun Kim[a,b], Min Chan Kim[a], Jin Suk Myung[b], Reza Salehiyan[c], Woo Jin Choi[b], and Kyu Hyun[a,*]